Failure Analysis in Dry Roll-Transferred Micro-LEDs with Limited Prior Knowledge

Jae-Hyun Kim and Chung-Seog Oh***
*Korea Institute of Machinery & Materials, Daejeon, Republic of Korea
**Kumoh National Institute of Technology, Gumi, Gyeongbuk, Republic of Korea

Abstract
This study analyzes micro-LEDs using focused ion beam milling and X-ray spectroscopy. Composed of GaN with six layers (39 × 44 μm²), defects like Kirkendall voids and misalignment cause failures. A 3D model was developed to aid future failure analysis, addressing high transfer costs in micro-LED displays.

Author Keywords
Alignment; Dry roll-transfer; Failure analysis; Focused ion beam; Micro-LED.

1. Introduction
Micro-LEDs (μLEDs) offer high resolution, contrast, color accuracy, and power efficiency, along with enhanced durability, making them ideal for next-generation displays [1]. However, commercialization remains challenging due to high transfer costs, which require the precise placement of millions of μLEDs (e.g., 25 million for a 4K TV) onto a backplane [2]. Various transfer methods have been proposed [3], but stress-induced damage often leads to defective pixels, necessitating process improvements. Finite element analysis (FEA) can help predict failures, yet it requires an accurate 3D model, something difficult to obtain, especially when μLED suppliers do not provide it.

This study employs a reverse engineering approach using focused ion beam (FIB) technology to analyze the geometry, internal (inter-layer) structure, material composition, and failure mechanisms of μLED devices with limited prior information, enabling the development of FEA models. Additionally, we identify key challenges that must be addressed to improve transfer yield.

2. Analysis of μLEDs with Limited Information
Overview of Target μLEDs: The operational status of green μLEDs, dry roll-transferred onto copper circuits, was evaluated by applying a DC voltage of 2.7 V. Two intact and bright (IAB) devices, one intact but dim (IBD) device, and one damaged and failed (DAF) device were selected. These were observed under a 50× optical microscope (Figure 1). Circuit geometry and dimensions were measured from optical images without μLEDs (Figure 2(a)) and illustrated in Figure 2(b). The geometry, internal structure, and material composition of identifiable μLED devices were analyzed using a dual-beam FIB system (Helios NanoLab 600, FEI) with SEM and FIB.

Planar Geometry Measurements: An ion beam image of the IAB1 device's top surface is shown in Figure 3(a). Using the microscope's software (or image analysis program), its planar dimensions were measured at 39.4 × 43.6 μm². The same method was applied to IAB2, IBD, and two undamaged devices (ETC1, ETC2), with results summarized in Table 1, revealing size variations. Based on these measurements, the μLED size was modeled as 39.0 × 44.0 μm² (Figure 3(b)). To clarify cross-sectional analysis, horizontal (H) and vertical (V) directions were defined in Figure 3(b).

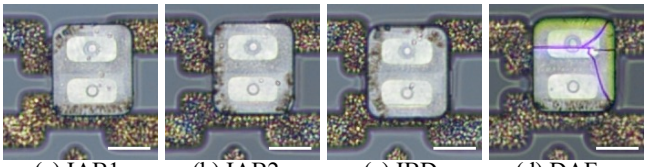

(a) IAB1 (b) IAB2 (c) IBD (d) DAF

Figure 1. Optical microscope images of three types of μLEDs roll-transferred by dry method (Scale bar: 20 μm).

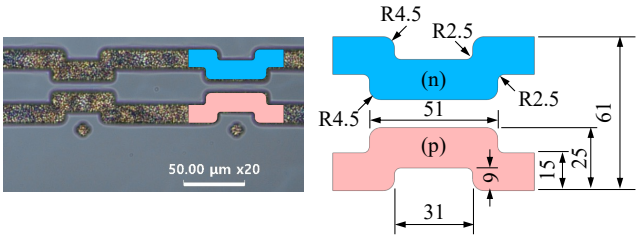

(a) Optical image (b) Planar dimension [μm]

Figure 2. Test backplane: Top blue is the cathode (n), bottom red is the anode (p).

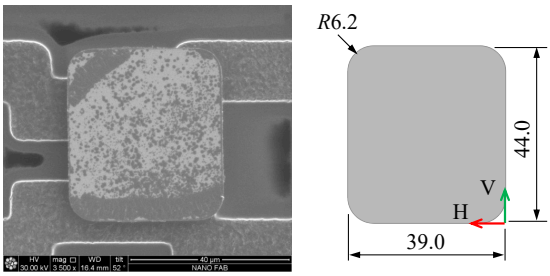

(a) Ion beam image (b) Planar model [μm]

Figure 3. Ion beam image of a μLED (IAB1) and dimensions of the top surface's planar model.

Table 1. Planar sizes of 5 different μLEDs [unit: μm]

μLED	l_H	l_V	R
IAB1	39.4	43.6	6.3
IAB2	38.2	43.9	6.0
IBD	38.3	44.3	6.3
ETC1	39.1	43.4	6.2
ETC2	38.5	44.1	6.3
Mean	38.7	43.9	6.2
SD	0.5	0.3	0.1

ISSN 0097-996X/25/5602-0825-$1.00 © 2025

Cross-Sectional Observation of Undamaged Devices: To examine the internal structure, the IAB1 μLED was analyzed along the V-axis. Ion milling at ~1 μm intervals (46 steps) provided cross-sectional images (Figure 4), revealing two electrodes connecting to the driving circuit. Figures 4(f)–(j) show a recessed groove in the cathode. The IAB2 device was then analyzed along the H-axis, with ion milling at 1–3 μm intervals (12 steps), and key cross-sections compiled in Figure 5. Observations from both axes clarified the layered structure and confirmed circular grooves in the cathodes.

Measurement of Layer Dimensions inside the Device: The lower-right section of Figure 4(c) (V ≈ 10 μm) was magnified (×20,000) and shown in Figure 6(a), where the thicknesses of three distinct layers (L1–L3) were measured. Since SEM images from FIB milling show projected depths (e), true thickness (l) was calculated using $l = e/\cos(38°)$ (Figure 6(b)). Measured values are annotated in Figure 6(a) as ***l***(*e*). The platinum (Pt) layer above L1 serves as a protective coating during FIB processing.

Next, the lower-right section of Figure 5(e) was magnified (×20,000) and presented in Figure 7(a). L5, the test copper circuit, measured 1.2 μm thick, while L4, connecting the μLED to the circuit, reached a maximum thickness of 1.4 μm. Figure 7(b) provides detailed views of L2 and L3, showing L2's alternating sub-layers: 400 nm (L21) and 100 nm (L22). The circular groove in the cathode was identified as a 1.2 μm-high contact hole.

Material Composition Analysis: To determine the materials in the dry-transferred μLED layers, energy-dispersive X-ray spectroscopy (EDS, Oxford) was conducted on the DAF device. The analysis targeted points along the cross-section at H = 18.4 μm (Figure 8). EDS results for the L3 layer measurement point are shown in Figure 9.

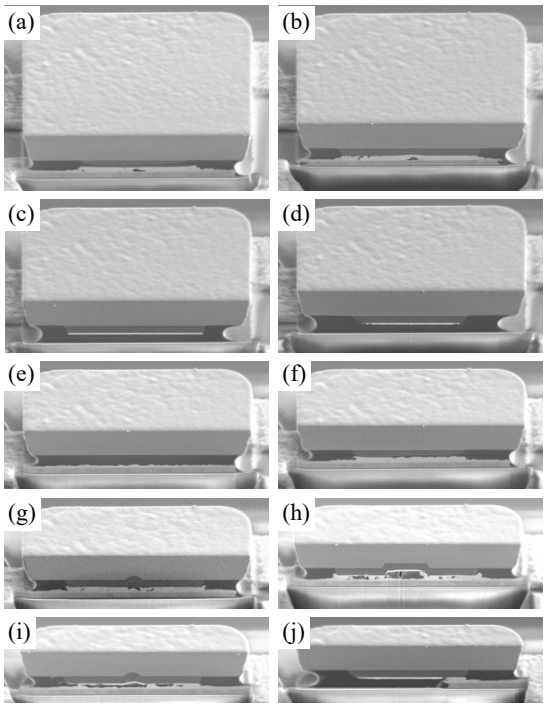

Figure 4. Cross-sectional images (x5,000) of IAB1 along the V direction at V [μm] values of (a) 4, (b) 6, (c) 12, (d) 17, (e) 26, (f) 28, (g) 32, (h) 38, (i) 42, (j) 43. (Scale bar: 10 μm).

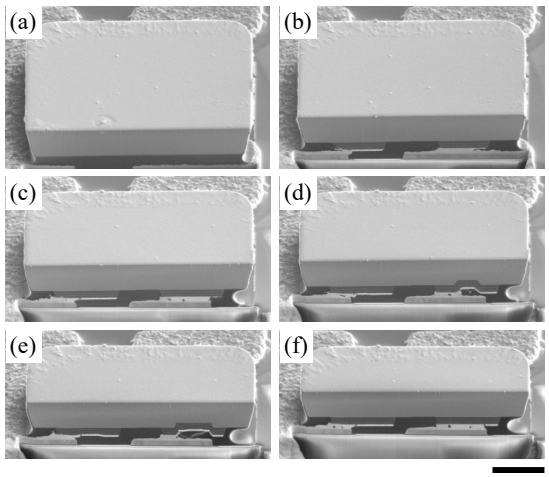

Figure 5. Cross-sectional images (×5,000) of IAB2 along the H direction at H = (a) 5, (b) 9, (c) 16, (d) 17, (e) 22, (f) 25 μm. (Scale bar: 10 μm)

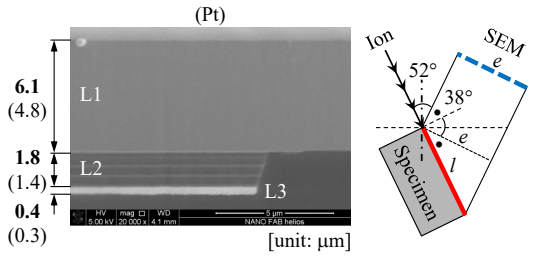

(a) Detailed cross-section of IAB1 (b) Ion beam angle

Figure 6. Layer thickness measurement from a cross-section before Figure 4(c).

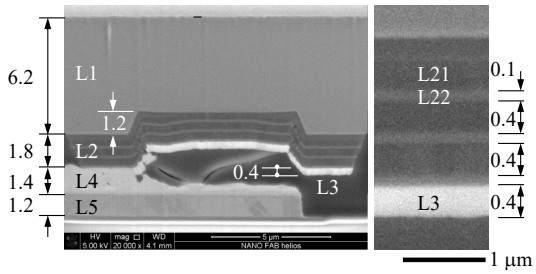

(a) Detailed cross-section of IAB2 (b) L2 layer

Figure 7. Cross-sectional image of all layers after dry transfer to reconfirm thicknesses of L1~L3, measure L4 and L5, and detail measurements of L2.

Multiple elements were detected, making it difficult to identify the predominant one. To clarify, composition analysis results are summarized in Table 2. EDS also accounted for surrounding elements (C, O, Si). The analysis confirmed the following compositions: L1 (GaN), L21 (Al), L22 (Ti), L3 (Au), L4 (lead-free solder), and L5 (Cu).

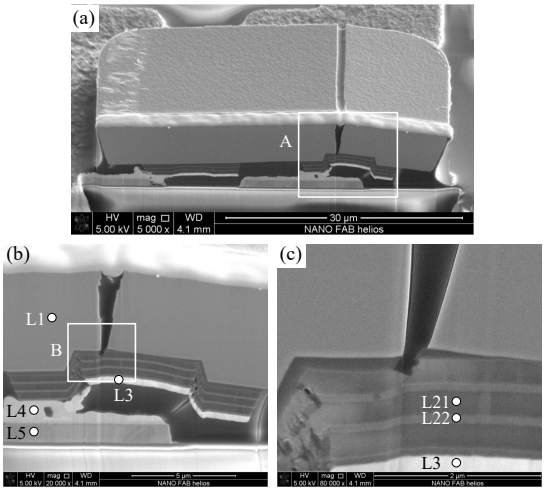

Figure 8. Cross-sectional SEM images indicating the EDS measurement locations for DAF: (a) Full view at H = 18.4 μm, (b) Enlarged view of rectangle A in (a), (c) Enlarged view of rectangle B in (b)

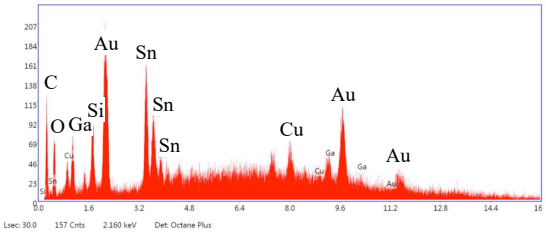

Figure 9. EDS analysis results at a measurement point in L3 layer, as indicated in Figures 8(b) and 8(c)

Table 2. EDS analysis results [unit: wt%]

Layer	Al	Au	C	Cu	Ga	N	O	Si	Sn	Ti
L1	-	-	2.2	-	**91.8**	**2.0**	2.2	1.9	-	-
L21	**24.9**	35.1	-	-	8.2	-	-	0.9	-	31.0
L22	**15.1**	23.0	1.3	-	12.0	-	5.6	0.9	-	**42.2**
L3	0.9	**82.3**	2.5	-	4.4	-	5.3	2.5	-	2.0
L4	0.8	**46.6**	1.7	**2.2**	4.7	-	4.0	2.0	**36.3**	1.8
L5	0.1	0.7	1.0	**88.9**	2.3	-	2.8	3.0	0.8	0.5

3. Reverse Engineering Results and 3D Model

Layer Structure and EDS Analysis Results: Through extensive cross-sectional observations using FIB and EDS analysis, the thickness and composition of the μLED device, driving circuit, and solder were identified. These results are summarized in Table 3.

3D Model Constructed via Reverse Engineering: A 3D model was constructed based on optical microscopy and FIB system observations, as shown in Figure 10. Additionally, a simulated model of the misaligned IAB2 device from Figure 1(b) is presented in Figure 11, along with the A-A cross-sectional view corresponding to Figure 5(e). The model closely resembles the cross-sectional features observed in the FIB analysis.

Table 3. Summary of the composition, thickness, and role of each layer

Layer	Mat'l	Thickness [μm]	Role
L1	GaN	6.2	μLED
L21	Al	0.4	Electrode
L22	Ti	0.1	Electrode
L3	Au	0.4	Electrode
L4	SAC	1.4 Max.	Lead-free solder
L5	Cu	1.2	Test circuit

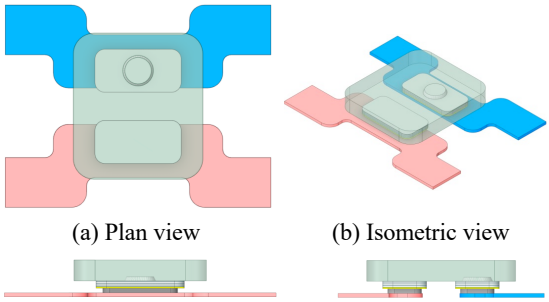

Figure 10. 3D unit model of μLED created through reverse engineering.

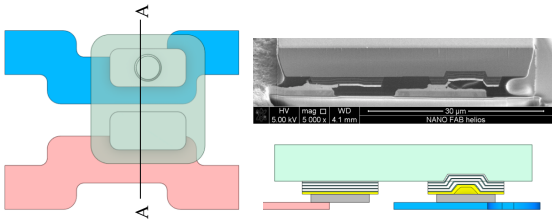

Figure 11. Misaligned 3D model (left) of IAB2 and comparison with FIB cross-section A-A (right)

4. Failure Analysis using FIB

As shown in Figure 1, although no external damage is visible, IAB2 and IBD show significant brightness differences under the same voltage. Their cross-sections were analyzed using FIB and compared in Figure 12. Figures 12(c) and 12(d) show no major differences in their flat electrodes, but Figures 12(e) and 12(f) reveal uneven solder in IBD, reducing its contact area. This likely results from irregular flux flow during solder reflow (see areas A and B in Figure 12).

Figure 13 shows a fully damaged IBD device due to pressure during dry transfer. In the magnified view of A region (Figure 13(a)), arrows in Figure 13(b) indicate Kirkendall voids [4] at the boundary, likely caused by differing diffusion rates of gold, solder, and copper atoms during reflow.

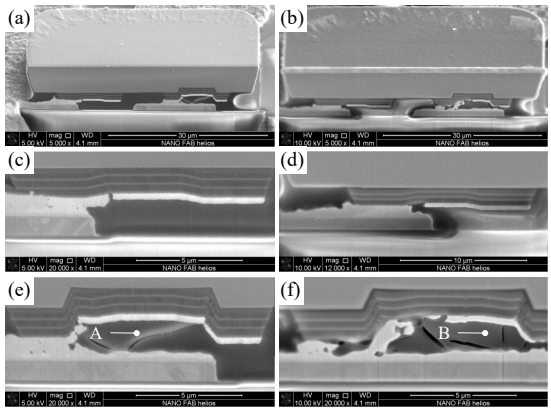

Figure 12. Cross-sectional images of a normal (a; IAB2) and a dim (b; IBD) μLED, along with their respective left and right enlarged images (c, e) and (d, f).

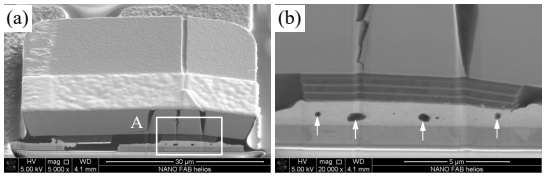

Figure 13. Cross-sectional SEM images for IBD: (a) Full view at H = 10 μm, (b) Enlarged view of rectangle A in (a).

5. Conclusion

This study utilized focused ion beam techniques to analyze the internal and external geometry and structure of μLED devices, which were then used to create 3D models for finite element analysis. The results reveal that the μLED device is made of GaN and consists of six distinct layers. Using this model, potential damage to the device during the transfer process can be minimized, thereby improving transfer yield. This research is expected to serve as foundational data for enhancing the μLED transfer process and facilitating its commercialization.

6. Acknowledgements

This work was supported by the Kumoh National Institute of Technology (2022–2024).

7. References

1. Chen D, Chen YC, Zeng G, Zhang DW, Lu HL. Integration technology of micro-LED for next-generation display. *Research*. 2023;6:0047.
2. Yu B, Li Y, Ding X, Li Z. Challenges of high-yield manufacture in micro-light-emitting diodes displays: chip fabrication, mass transfer, and detection. *J Phys D Appl Phys*. 2024;57(46):463001.
3. Cao C, Sun Y. Transfer printing technologies and applications. *Mater Today*. 2024; Available from: Elsevier.
4. Wang J, Chen J, Zhang L, Zhang Z, Han Y, Hu Z, et al. Forming mechanism and growth of Kirkendall voids of Sn/Cu joints for electronic packaging: A recent review. *J Adv Joining Process*. 2022;6:100125.